Available online at www.sciencedirect.com
ScienceDirect
International Journal of Thermal Sciences 45 (2006) 1205–1212
International Journal of Thermal Sciences
www.elsevier.com/locate/ijts

Film condensation in horizontal microchannels: Effect of channel shape ☆

Hua Sheng Wang *, John W. Rose

Department of Engineering, Queen Mary, University of London, London E1 4NS, UK

Received 30 August 2005; accepted 18 March 2006

Available online 27 April 2006

Abstract

The paper gives a progress report on a theoretical study of film condensation in microchannels. The model takes account of surface tension, vapor shear stress and gravity. The effect of channel shape is investigated for condensation of R134a in channels with cross sections: square, triangle, inverted triangle, rectangle with longer side vertical, rectangle with longer side horizontal and circle. The case considered here is where the channel wall temperature is uniform and the vapor is saturated at inlet. For a given mass flux, the local condensate film profile around the cross section is calculated together with the mean heat-transfer coefficient at different distances along the channel. Results are presented here for one vapor mass flux, one vapor temperature and one wall temperature.

Keywords: Condensation; Heat transfer enhancement; Microchannel; Non-circular tube; Theory; Surface tension; R134a

1. Introduction

Microchannels are increasingly used to improve heat-transfer performance and to enable compact geometries. For condensation, owing to surface tension effects, methods used to treat larger channels are not suitable when the channel dimension is around 1 mm or less. Recent experimental and modelling work on condensation in small channels has been reviewed by Cavallini et al. [1,2] and Bandhauer et al. [3]. In many of the earlier heat-transfer measurements the vapor-side, heat-transfer coefficients are based on overall measurements using "Wilson plots" or coolant-side correlations and consequently have large uncertainty. Notable exceptions, in which the wall temperature was measured directly, are the works of Koyama et al. [4,5] and Cavallini et al. [6,7]. Available empirical and semi-empirical models underpredict these data except at the lowest vapor mass fluxes.

An important mechanism of heat transfer enhancement during condensation in non-circular microchannels is the surface tension generated transverse pressure gradient in the condensate film. This leads to condensate flow towards the corners and thins the film along the sides of the channel giving rise to high heat-transfer and condensation rates. The transverse pressure gradient arises from variation of condensate surface curvature along the side of the channel.

The present work relates to condensation in horizontal square, rectangular, triangular and circular microchannels and concentrates here on channel shape. Preliminary results have been reported earlier (Wang et al. [8], Wang and Rose [9–13]). The overall objective of the research program is to establish methods for determination of the optimum channel shape, dimensions and size for given duty.

2. Theoretical model

The model includes surface tension and surface curvature effects along with a Nusselt approach for the condensate film, that is, laminar flow neglecting of inertia and convection terms. A detailed description of the theory and calculation method is given by Wang and Rose [12]. Fig. 1 shows the co-ordinate systems used for the sides (Cartesian: $0 \leqslant x \leqslant x_a$, $x_b \leqslant x \leqslant x_c$ and $x_d \leqslant x \leqslant x_m$ for square/rectangular section; $x_a \leqslant x \leqslant x_b$ and $x_c \leqslant x \leqslant x_m$ for triangular section) and for the corners (polar: $x_a \leqslant x \leqslant x_b$ and $x_c \leqslant x \leqslant x_d$ for square/rectangular section, $0 \leqslant x \leqslant x_a$ and $x_b \leqslant x \leqslant x_c$ for triangular section, $0 \leqslant x \leqslant x_m$

☆ A preliminary version of this paper was presented at ICMM05: Third International Conference on Microchannels and Minichannels, held at University of Toronto, June 13–15, organized by S.G. Kandlikar and M. Kawaji, CD-ROM Proceedings, ISBN: 0-7918-3758-0, ASME, New York.

* Corresponding author.
E-mail addresses: h.s.wang@qmul.ac.uk (H.S. Wang), j.w.rose@qmul.ac.uk (J.W. Rose).

1290-0729/$ – see front matter
doi:10.1016/j.ijthermalsci.2006.03.004

Nomenclature

b	side length of triangular and square channels
d	diameter of circular section channel
f	friction factor modified to account for "suction"
f_v	friction factor of vapor flow without surface transpiration, $\tau_v/\frac{1}{2}\rho_v U_v^2$
f_ϕ, f_τ, f_z	see Eqs. (5)–(7)
g	specific force of gravity
h	height of rectangle
h_{fg}	specific enthalpy of evaporation
P_v	vapor pressure
q	heat flux
r_c	radius of curvature of the condensate surface in the channel cross-section, see Fig. 1
r	radial polar co-ordinate, see Fig. 1
r_i	distance from origins O_1, O_2 to vapour–liquid interface, see Fig. 1
r_w	radius of curvature of channel surface in the channel cross-section, see Fig. 1
T	temperature
T_s	saturation temperature
T_w	tube wall temperature
T^*	reference temperature, see Eq. (14)
u	condensate velocity along channel surface in x-direction or ϕ direction, see Fig. 1
U_v	local bulk vapor velocity
v	condensate velocity along channel surface in z-direction, see Fig. 1
w	width of rectangle
x, y	coordinates along and normal to channel surface, see Fig. 1
x_a, x_b, x_c, x_d	x coordinates at the foot of the perpendicular from origins O_1 and O_2, see Fig. 1
x_m	x coordinate at centre of bottom surface, see Fig. 1
X, Y	fixed coordinates defined in Fig. 1
z	coordinate down stream, see Fig. 1

Greek symbols

α_x	local heat-transfer coefficient
α_z	average heat-transfer coefficient over perimeter of channel at location z
δ	condensate film thickness, defined in Fig. 1
λ	condensate thermal conductivity
χ	vapor quality
ν	kinematic viscosity
ρ	density
σ	surface tension
τ_i	vapor shear stress at vapor–liquid interface
τ_v	vapor shear stress at surface without transpiration
ϕ	angle, polar co-ordinate, see Fig. 1
$\phi_a, \phi_b, \phi_c, \phi_d$	angles corresponding to x_a, x_b, x_c, x_d see Fig. 1
ϕ	see Eq. (10)
ψ	angle between the normal of channel surface and Y coordinate, see Fig. 1

Subscripts

i	interface
l	condensate
s	saturation
v	vapor
w	wall
x	local
z	average at the location, z-direction
φ	φ direction
τ	τ component

for circular section). Conservation of mass, momentum and energy for the condensate film lead to the following equations for the local condensate film thickness δ:

$$\frac{(\rho_l-\rho_v)g}{3\nu_l}\frac{\partial}{\partial x}\left(\delta^3\sin\psi\right)+\frac{\sigma}{3\nu_l}\frac{\partial}{\partial x}\left\{\delta^3\frac{\partial}{\partial x}\left(\frac{1}{r_c}\right)\right\}+\frac{1}{2\nu_l}\frac{\partial(\tau_i\delta^2)}{\partial z}-\frac{1}{3\nu_l}\frac{\partial}{\partial z}\left(\delta^3\frac{dP_v}{dz}\right)=\frac{1}{(1+\zeta\lambda_l/\delta)}\frac{\lambda_l(T_s-T_w)}{h_{fg}\delta} \tag{1}$$

where

$$\frac{1}{r_c}=\frac{\partial^2\delta/\partial x^2}{\{1+(\partial\delta/\partial x)^2\}^{3/2}} \tag{2}$$

used when considering channel sides and

$$\frac{(\rho_l-\rho_v)g}{3\nu_l}\frac{\partial}{r\partial\varphi}\left[\delta f_\varphi(\delta)\sin\varphi\right]+\frac{\sigma}{3\nu_l}\frac{\partial}{r\partial\varphi}\left[\delta f_\varphi(\delta)\frac{\partial}{r\partial\varphi}\left(\frac{1}{r_c}\right)\right]+\frac{1}{\nu_l}\frac{\partial}{\partial z}\left[\delta f_\tau(\delta)\tau_i\right]+\frac{1}{4\nu_l}\frac{\partial}{\partial z}\left[\delta f_z(\delta)\frac{dP_v}{dz}\right]=\frac{1}{1+\frac{\zeta\lambda_l}{r_w\ln[r_w/(r_w-\delta)]}}\frac{\lambda_l(T_s-T_w)}{h_{fg}r_w\ln[r_w/(r_w-\delta)]} \tag{3}$$

where

$$\frac{1}{r_c}=\frac{r_i^2+2(\partial r_i/\partial\varphi)^2-r_i(\partial^2 r_i/\partial\varphi^2)}{\{r_i^2+(\partial r_i/\partial\varphi)^2\}^{3/2}} \tag{4}$$

$$f_\varphi(\delta)=-r_w^2+r_w\delta-\frac{\delta^2}{3}+\left(r_w-\frac{\delta}{2}\right)(r_w-\delta)\frac{2+(\frac{r_w}{r_w-\delta})^3}{1+(\frac{r_w}{r_w-\delta})^2}-\frac{r_w^2(r_w-\delta)}{\delta}\frac{2-(\frac{r_w}{r_w-\delta})}{1+(\frac{r_w}{r_w-\delta})^2}\ln\left(\frac{r_w}{r_w-\delta}\right) \tag{5}$$

$$f_\tau(\delta)=(r_w-\delta)\left[1+\frac{(r_w-\delta)}{\delta}\ln\left(\frac{r_w-\delta}{r_w}\right)\right] \tag{6}$$

$$f_z(\delta)=-r_w\delta+\frac{\delta^2}{3}+2(r_w-\delta)^2\times\left[1+\frac{(r_w-\delta)}{\delta}\ln\left(\frac{r_w-\delta}{r_w}\right)\right] \tag{7}$$

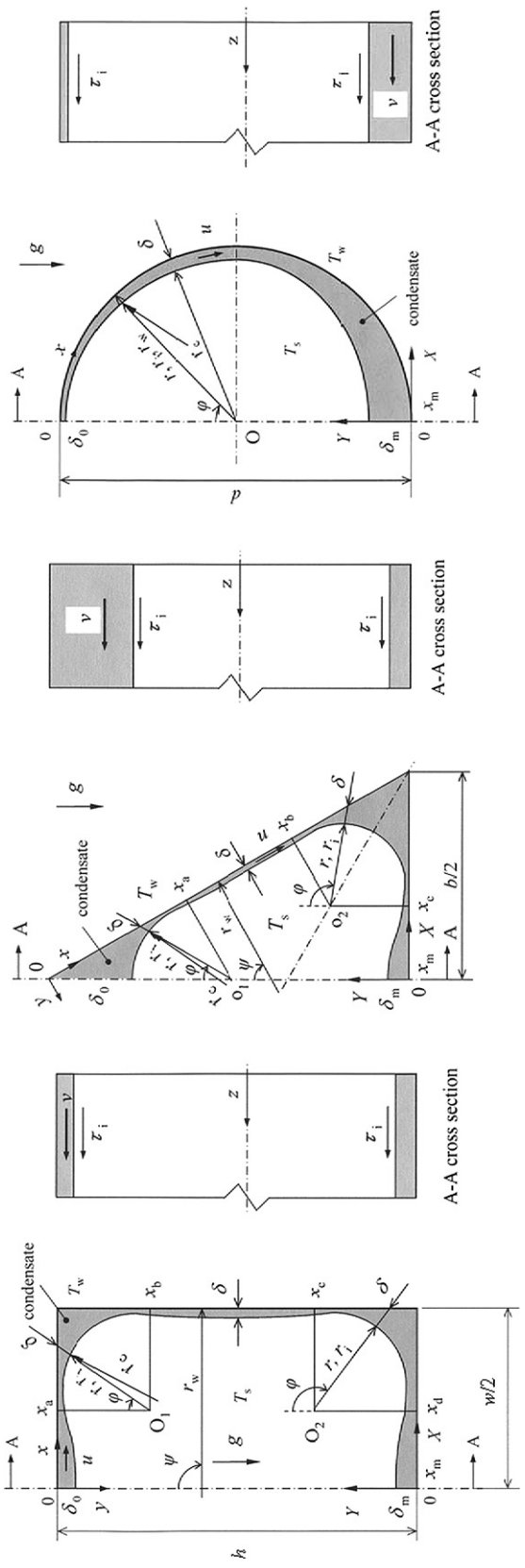

Fig. 1. Physical model and coordinates.

used when considering the neighborhood of corners and for the circular section channel. (Note that the parameter ζ in Eq. (1) and results from the interface "temperature jump" which is negligible in this present case, see Wang and Rose [12].)

The four boundary conditions in the section of the channel are provided by the condition that odd derivates (1st and 3rd) with respect to x or φ are zero at points of symmetry (top of upright triangular section or middle of upper and lower horizontal sides) and for the case of saturation conditions at the inlet (considered here) the necessary further boundary condition is that the film thickness is zero everywhere at the inlet, $z = 0$.

The effect of condensation (suction) is taken into account by using the approach suggested by Mickley et al. [14] for flow over a flat plate with suction and described in Kays et al. [15]. This method was also used to treat condensation in tube by Cavallini et al. [16]. The interfacial surface shear stress is

$$\tau_{\mathrm{i}} = \frac{1}{2} f \rho_{\mathrm{v}} U_{\mathrm{v}}^2 \tag{8}$$

where

$$f = \frac{\phi}{e^{\phi} - 1} f_{\mathrm{v}} \tag{9}$$

$$\phi = -\frac{2m}{f_{\mathrm{v}} \rho_{\mathrm{v}} U_{\mathrm{v}}} \tag{10}$$

m is the condensation flux, f_{v} is the single-phase friction factor obtained by the Churchill equation [17]. Here we take U_{v} as the local vapor velocity which is calculated from the inlet mass flow minus the condensation rate up to the position in question.

At a given location z along the channel, the local heat-transfer coefficient α_x is defined as

$$\alpha_x = q/(T_{\mathrm{s}} - T_{\mathrm{w}}) = \frac{1}{1 + \zeta \lambda_l / \delta} \frac{\lambda_l}{\delta} \tag{11}$$

for the sides and

$$\alpha_x = q/(T_{\mathrm{s}} - T_{\mathrm{w}}) = \frac{1}{1 + \frac{\zeta \lambda_l}{r_{\mathrm{w}} \ln[r_{\mathrm{w}}/(r_{\mathrm{w}} - \delta)]}} \frac{\lambda_l}{r_{\mathrm{w}} \ln[r_{\mathrm{w}}/(r_{\mathrm{w}} - \delta)]} \tag{12}$$

for the corners.

The average heat-transfer coefficient α_z for the section at a given distance z along the channel is found by integrating the heat transfer around the channel section location to obtain the mean heat flux at z, then

$$\alpha_z = q_z/(T_{\mathrm{s}} - T_{\mathrm{w}}) \tag{13}$$

T_{s} and T_{w} are here uniform along the channel.

3. Results and discussion

Results are presented below for condensation of R134a in square (side 1 mm), triangular (side 1 mm), rectangular (sides 1 mm × 1.5 mm, both orientation) and circular (diameter 1 mm) channels. Calculated condensate profiles in various channels are shown in Figs. 2–7. In all cases the mass flux (mass velocity) of the refrigerant was 500 kg m^{-2} s, the vapor temperature was 50 °C and the surface temperature was 44 °C taken here to

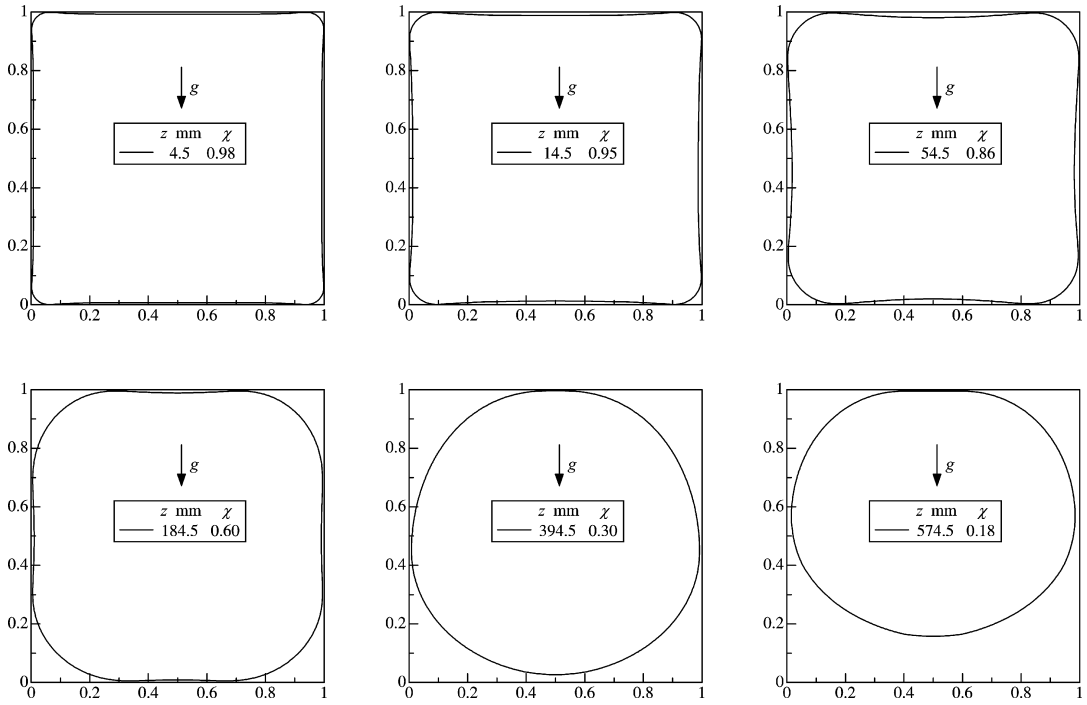

Fig. 2. Condensate film profiles along channel surface at different distances for square cross-section channel ($b = 1.0$ mm).

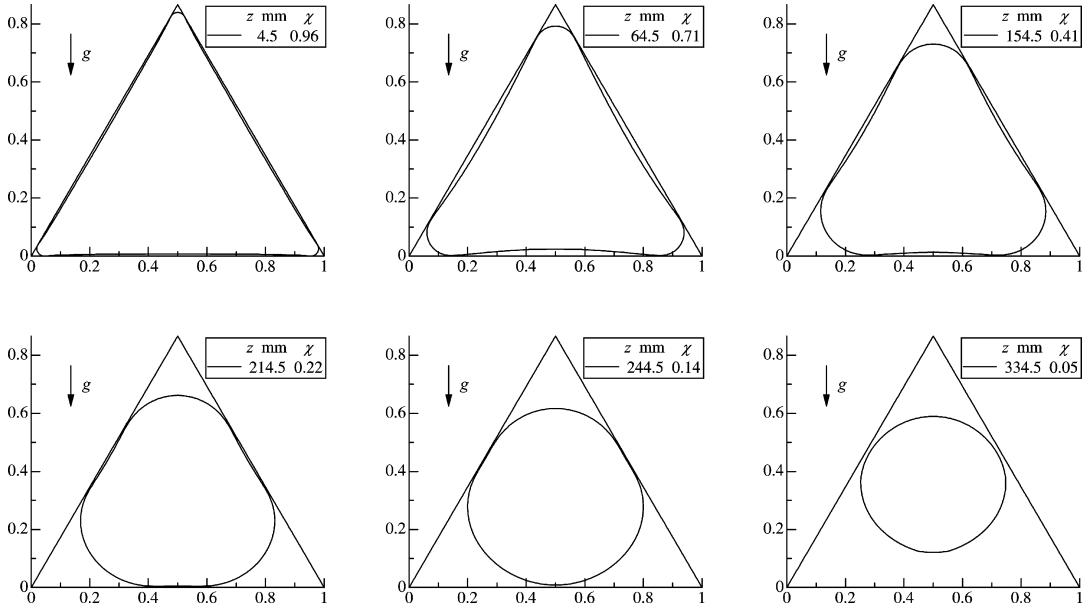

Fig. 3. Condensate film profiles along channel surface at different distances for triangular cross-section (vertex up) channel ($b = 1.0$ mm).

be constant along the channel. The physical properties of the refrigerants were obtained from NIST REFPROP Version 6 [18]. Condensate properties were taken to be uniform at reference temperature

$$T^* = \frac{1}{3}T_s + \frac{2}{3}T_w \tag{14}$$

and σ and h_{fg} were obtained at T_s.

For the square channel (Fig. 2) very thin condensate film regions are seen near the corners towards the channel entrance. It is also seen that the thin film persists and covers an increasing portion of the upper surface for distances z along the channel exceeding 400 mm. For the triangle with vertex up (Fig. 3) there is no clear effect of gravity and no thin film for $z > 300$ mm. When the vertex of the triangular channel is down (Fig. 4) the lower part begins to fill (stratified flow) at around $z = 250$ mm but a thin film region persists on the upper horizontal surface. For the rectangular channel with long side horizontal (Fig. 5) the film in the centre of the upper surface remains relatively thick. When the long side is vertical (Fig. 6) for $z > 500$ mm there is no thin film on the upper surface and only small thin

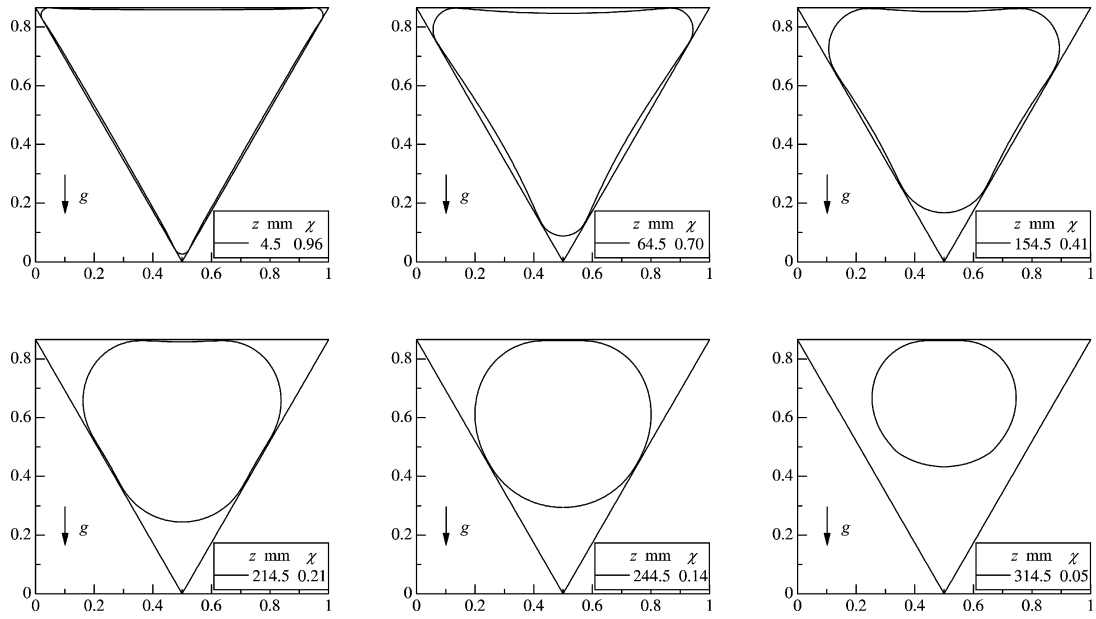

Fig. 4. Condensate film profiles along channel surface at different distances for triangular cross-section (vertex down) channel ($b = 1.0$ mm).

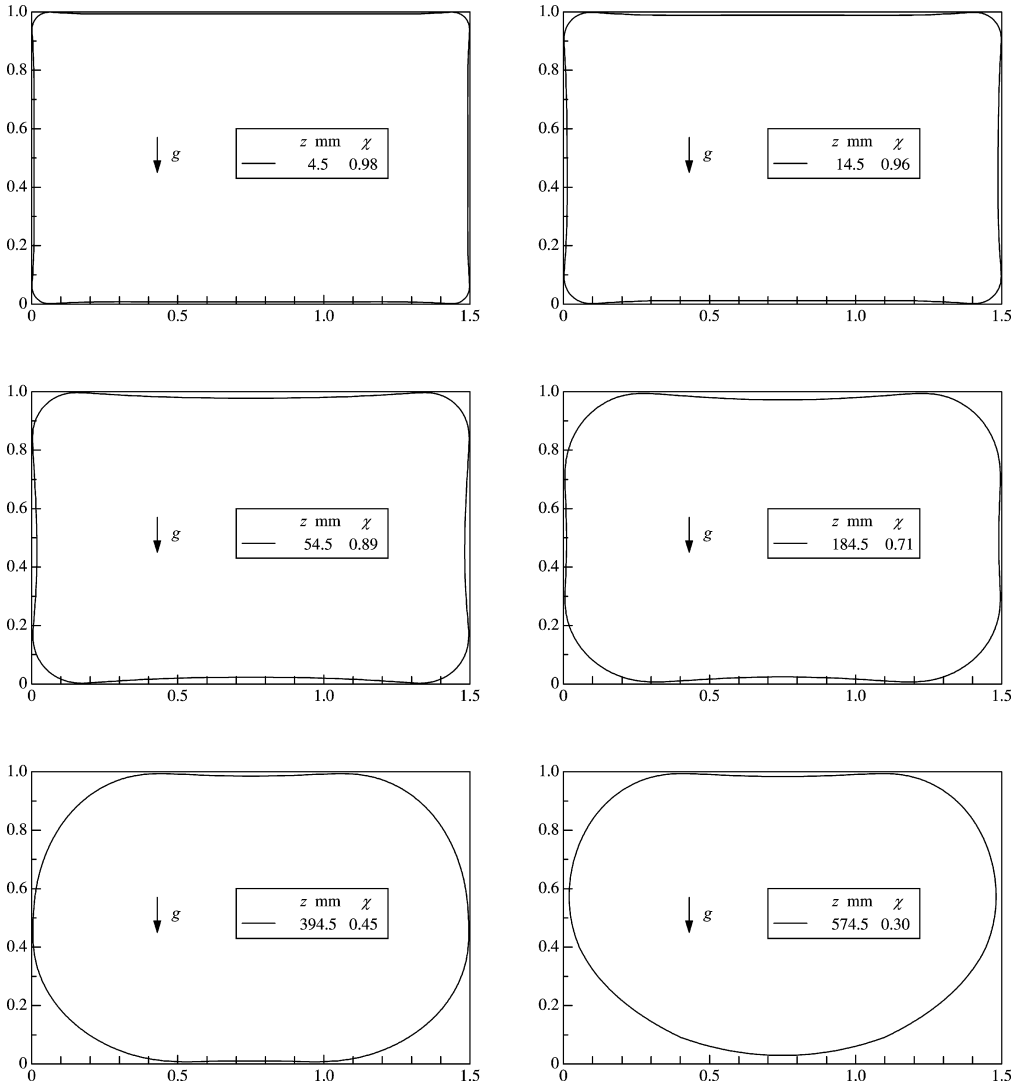

Fig. 5. Condensate film profiles along channel surface at different distances for rectangular cross-section (long side horizontal) channel ($w = 1.5$ mm, $h = 1.0$ mm).

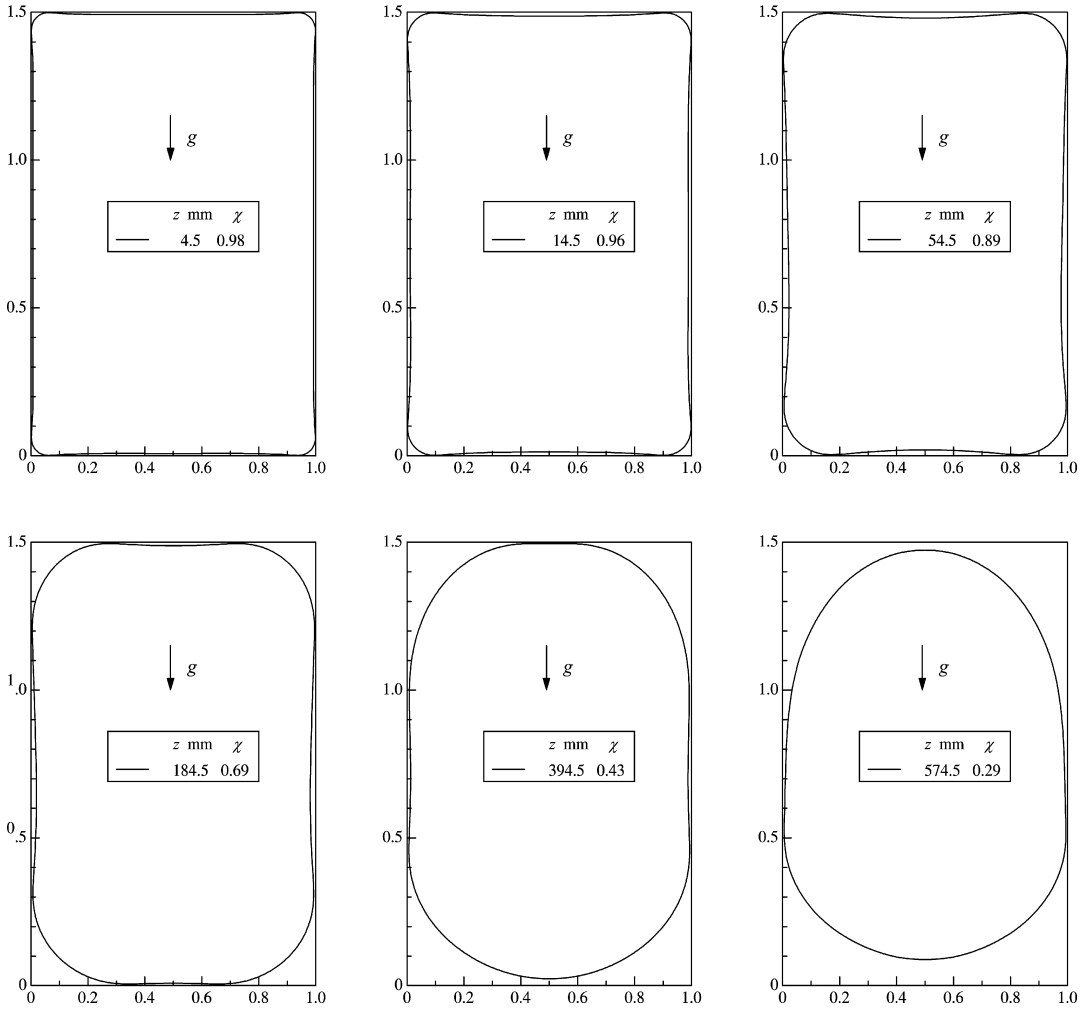

Fig. 6. Condensate film profiles along channel surface at different distances for rectangular (long side vertical) cross-section channel ($w = 1.0$ mm, $h = 1.5$ mm).

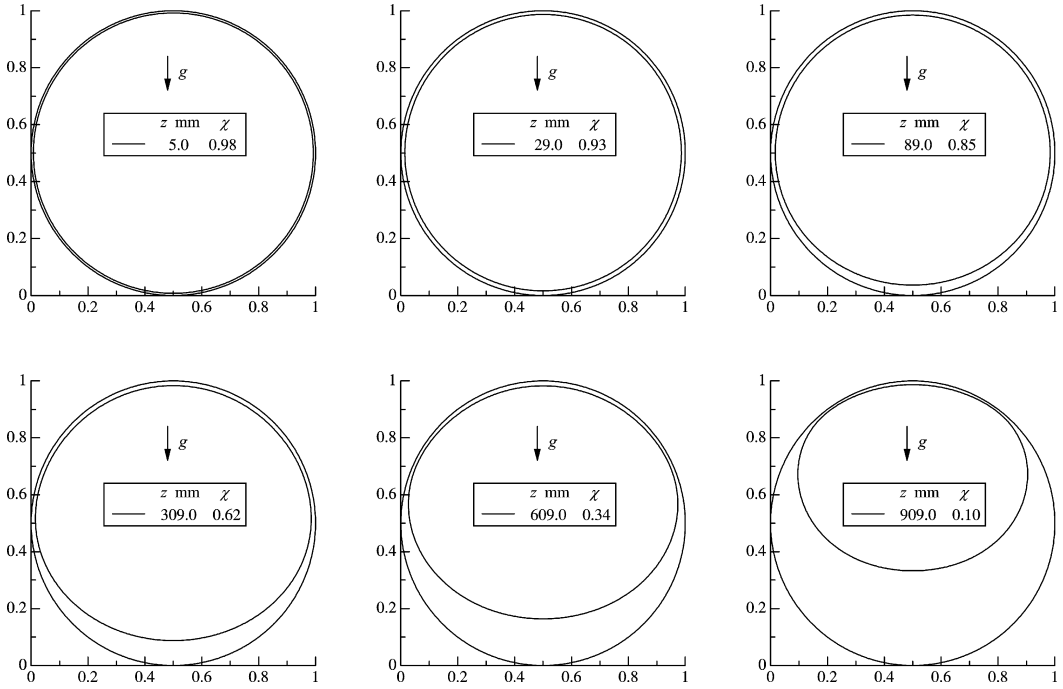

Fig. 7. Condensate film profiles along channel surface at different distances for circular cross-section channel ($d = 1.0$ mm).

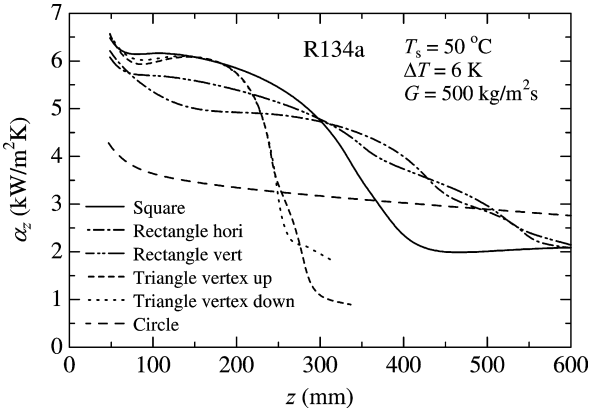

Fig. 8. Variation of average heat-transfer coefficient along the channels.

film regions on the lower halves of the vertical sides. For the circular channel (Fig. 7) there is no thin film region except at the furthest distance along the channel due to the stronger change in condensate surface curvature where the relatively thin film on the upper surface blends with the accumulation of condensation in the lower part of the channel.

Fig. 8 shows the variation along the channel of the mean (around the channel perimeter) heat-transfer coefficients for the same conditions. For the case considered, where the saturated vapor at inlet encounters the channel wall at a lower temperature, the heat-transfer coefficient falls rapidly over the first 40 mm or so from infinity at inlet to the levels shown. The results in this range are omitted on Fig. 8 but shown in earlier papers (Wang et al. [8], Wang and Rose [9–13]).

For the triangular channels the heat-transfer coefficient falls abruptly from a steady value of a little over 6 kW m^{-2} K^{-1} at a distance of approximately 200 mm along the channel as the channel becomes "flooded". For the vertex down case the fall in coefficient is less owing to the persistence of thin film on the upper horizontal surface (see Fig. 4). For the square channel the heat-transfer coefficient near the inlet is a little higher and falls off less steeply owing to the larger channel perimeter and even increases slightly at further distances owing to persistence of thin film on the upper surface of the channel (see Fig. 2). For the rectangular section channels the fall off in coefficient is more continuous and gradual. The value near the inlet is around 5.5 kW m^{-2} K^{-1} when the longer side is vertical and around 5 kW m^{-2} K^{-1} when the longer side is horizontal. For the circular section channel, for which surface tension has negligible effect, the coefficient falls from around 4 kW m^{-2} K^{-1} to a little less than 3 kW m^{-2} K^{-1}. The non-circular channels all perform better than the circular channel near the inlet. This leads to increased condensate loading further along the channels where the coefficients fall, in all cases, below those of the circular channel. The relative importance of surface tension, gravity and vapor shear stress are discussed by Wang and Rose [11–13].

4. Concluding remarks

Full details of the model are given in (Wang and Rose [12]). The results and trends presented here and discussed above relate to only one fluid, to specific geometries and one mass flux condition. Before exploring a wider range of parameters the model will be improved. In particular, provision will be made for superheated vapor at inlet; modifications will be made to take account of variation of wall temperature. Comparisons will be made with experimental data.

Acknowledgements

This work was supported by the Engineering and Physical Sciences Research Council (EPSRC) of the UK through grants GR/S07209/01 and GR/S20345/01.

References

[1] A. Cavallini, G. Censi, D. Del Col, L. Doretti, A.G. Longo, L. Rossetto, Condensation heat transfer and pressure drop inside channels for AC/HP application, in: Proc. 12th Int. Heat Transfer Conference, Grenoble, France, August 18–23, vol. 1, 2002, pp. 171–186.

[2] A. Cavallini, L. Doretti, M. Matkovic, L. Rossetto, Update on condensation heat transfer and pressure drop inside microchannels, in: Proc. 3rd Int. Conf. on Microchannels and Minichannels, ASME, Toronto, Canada, 2005, CD, Paper ICMM 2005-75081.

[3] T.M. Bandhauer, A. Akhil, S. Garimella, Measurement and modeling of condensation heat transfer coefficients in circular microchannels, in: Proc. 3rd Int. Conf. on Microchannels and Minichannels, ASME, Toronto, Canada, 2005, CD, Paper ICMM 2005-75248.

[4] S. Koyama, K. Kuwahara, K. Nakashita, K. Yamamoto, Condensation of refrigerant R134a in a multiport channel, in: Proc. 1st Int. Conf. on Microchannels and Minichannels, ASME, Rochester, NY, April 24–25, 2003, pp. 193–205.

[5] S. Koyama, K. Kuwahara, K. Nakashita, K. Yamamoto, An experimental study on condensation of refrigerant R134a in a multiport extruded tube, Int. J. Refrigeration 26 (2003) 425–432.

[6] A. Cavallini, G. Censi, D. Del Col, L. Doretti, A.G. Longo, L. Rossetto, C. Zilio, Experimental investigation on condensation heat transfer coefficient inside multi-port channels, in: Proc. 1st Int. Conf. on Microchannels and Minichannels, ASME, Rochster, NY, April 24–25, 2003, pp. 691–698.

[7] A. Cavallini, D. Del Col, L. Doretti, M. Matkovic, L. Rossetto, C. Zilio, Condensation heat transfer inside multi-port minichannels, in: Proc. 2nd Int. Conf. on Microchannels and Minichannels, ASME, Rochester, NY, 2004, pp. 625–632.

[8] H.S. Wang, J.W. Rose, H. Honda, A theoretical model of film condensation in square section microchannels, Trans. IChemE, Chem. Eng. Res. Design 82 (A4) (2004) 430–434.

[9] H.S. Wang, J.W. Rose, Condensation in microchannels, in: Proc. 6th Int. Symp. on Heat Transfer, Beijing, China, June 15–19, 2004, pp. 22–31.

[10] H.S. Wang, J.W. Rose, Film condensation in horizontal triangular section microchannels, in: Proc. 2nd Int. Conf. on Microchannels and Minichannels, ASME Rochester, New York, 2004, pp. 661–666.

[11] H.S. Wang, J.W. Rose, Film condensation in horizontal microchannels: Effect of channel shape, in: Proc. 3rd Int. Conf. on Microchannels and Minichannels, ASME, Toronto, Canada, 2005, CD, Paper ICMM 2005-75260.

[12] H.S. Wang, J.W. Rose, A theory of film condensation in horizontal noncircular section microchannels, Trans. ASME J. Heat Transfer 127 (10) (2005) 1096–1105.

[13] H.S. Wang, J.W. Rose, Film condensation in horizontal circular-section microchannels, in: 5th Int. Symp. on Multiphase Flow, Heat Transfer and Energy Conversion, Xi'an, China, 3–6 July, 2005, Paper No. 370.

[14] H.S. Mickley, R.C. Ross, A.L. Squyers, W.E. Stewart, Heat, mass and momentum transfer for flow over a flat plate with blowing or suction, Rep. No. NACA-TN-3208, 1954.

[15] W.M. Kays, M.E. Crawford, B. Weigand, Convective Heat and Mass Transfer, fourth ed., McGraw-Hill, New York, 2005, pp. 212–215.

[16] A. Cavallini, D. Del Col, L. Doretti, G.A. Longo, L. Rossetto, A new computational procedure for heat transfer and pressure drop during refrigerant condensation inside enhanced tubes, J. Enhanced Heat Transfer 6 (1999) 441–456.

[17] S.W. Churchill, Friction-factor equation spans all fluid-flow regimes, Chem. Engrg. 84 (1977) 91–92.

[18] NIST Thermodynamic and transport properties of refrigerants and refrigerants mixtures – REFPROP, Version 6.0.